25. We thank the Egyptian Geological Survey and Mining Authority and Mme. Ferial El Bedewi, director of the Cairo Geological Museum, for support of field work. A. A. Barakat, A. A. Abd Ellatif, and W. J. Sanders helped in the field and Y. Attia and P. Chatrath provided logistical support. We thank D. C. Fisher for help in interpreting the locking knee, and P. Webb for information on swimming in anguilliform vertebrates. We thank F. Ankel-Simons, L. G. Barnes, D. L. Domning, D. C. Fisher, C. Gans, P. Myers, C. Ray, G. R. Smith, and F. C. Whitmore for reading the manuscript. Specimens were prepared by W. J. Sanders and illustrated by B. Miljour. Field research in Egypt in 1987 and 1989 was supported by the Duke University Fayum Expedition and by the National Geographic Society Committee on Research and Exploration (grants 3424-86 and 4154-89).

11 January 1990; accepted 25 April 1990

Solution Structure of the Glucocorticoid Receptor DNA-Binding Domain

TORLEIF HÄRD,* EDWIN KELLENBACH, ROLF BOELENS, BONNIE A. MALER, KARIN DAHLMAN, LEONARD P. FREEDMAN,† JAN CARLSTEDT-DUKE, KEITH R. YAMAMOTO, JAN-ÅKE GUSTAFSSON, ROBERT KAPTEIN‡

The three-dimensional structure of the DNA-binding domain (DBD) of the glucocorticoid receptor has been determined by nuclear magnetic resonance spectroscopy and distance geometry. The structure of a 71-residue protein fragment containing two "zinc finger" domains is based on a large set of proton-proton distances derived from nuclear Overhauser enhancement spectra, hydrogen bonds in previously identified secondary structure elements, and coordination of two zinc atoms by conserved cysteine residues. The DBD is found to consist of a globular body from which the finger regions extend. A model of the dimeric complex between the DBD and the glucocorticoid response element is proposed. The model is consistent with previous results indicating that specific amino acid residues of the DBD are involved in protein-DNA and protein-protein interactions.

THE GLUCOCORTICOID RECEPTOR belongs to a family of ligand-inducible nuclear transcription factors that include the steroid hormone, thyroid hormone, retinoic acid, and vitamin D_3 receptors. All members of this superfamily contain a highly conserved DNA-binding domain that consists of about 70 residues and mediates specific binding to hormone response elements on DNA (*1*). Protein fragments containing the glucocorticoid receptor DBD expressed in *Escherichia coli* exhibit sequence-specific binding to glucocorticoid response elements (GREs) (*2*, *3*). These protein fragments contain two zinc atoms, tetrahedrally coordinated by conserved cysteine residues, that are required for proper folding and DNA binding (*2*). The presence of zinc-binding domains is reminiscent of the "zinc finger" motif found in *Xenopus* TFIIIA (*4*), as well as similar domains found in retroviral nucleic acid binding proteins (*5*). However, the hormone receptor zinc-coordinating regions are not homologous to these other zinc fingers, suggesting that the DNA-binding domain of the steroid and thyroid hormone receptors constitutes a distinctive structural motif (*6*).

We have studied two protein fragments containing the glucocorticoid receptor DBD using two-dimensional nuclear magnetic resonance (2D NMR) and distance geometry (DG). These fragments contain 93 and 115 residues, respectively, with a common sequence encompassing the Cys^{440} to Ile^{519} and Cys^{421} to Ile^{500} segments of the rat and human glucocorticoid receptors, respectively (*7*, *8*). The structural studies focus on the 71-residue segment Cys^{440} to Arg^{510}, which includes the two zinc-coordinating finger regions (Fig. 1). Sequence-specific assignments of more than 90% of all observable ^1H resonances within this segment were obtained with the use of 2D double quantum filtered correlated spectroscopy (DQF-COSY), homonuclear Hartmann-Hahn spectroscopy (HOHAHA), and nuclear Overhauser enhancement spectroscopy (NOESY). The resonance assignments (*9*) were carried out with the use of well-established procedures (*10*, *11*).

Several elements of secondary structure within the Cys^{440} to Arg^{510} segment could be identified based on characteristic patterns of NOE connectivities (*10*). These elements include two α-helical regions encompassing Ser^{459} to Glu^{469} and Pro^{493} to Gly^{504}, a type I reverse turn between residues Arg^{479} to Cys^{482}, a type II reverse turn between residues Leu^{475} to Gly^{478}, a short stretch of antiparallel β sheet involving residues Cys^{440} and Leu^{441} and Leu^{455} to Cys^{457}, as well as

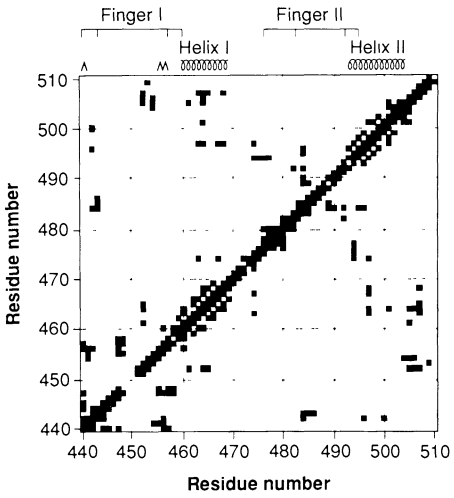

Fig. 2. Diagonal plot indicating residues between which NOEs have been found. Secondary structure elements and zinc coordination within the two finger domains (*19*) has also been indicated.

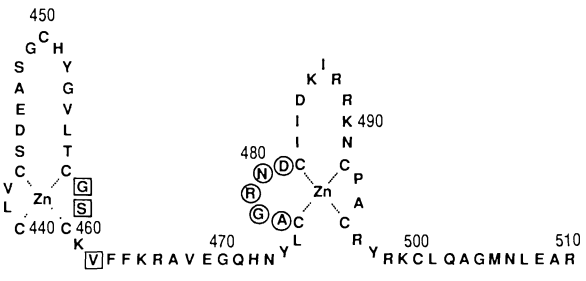

Fig. 1. The segment Cys^{440} to Arg^{510} of the rat glucocorticoid receptor DNA-binding domain (Cys^{421} to Arg^{491} of the human glucocorticoid receptor) for which the three-dimensional structure is presented here (*8*). The boxed residues indicate amino acids that are essential for discrimination between glucocorticoid and oestrogen response elements (GRE and ERE) (*26*). The circled residues indicate the segment that is important for protein-protein interactions in the dimeric DBD-GRE complex (*25*).

T. Härd, E. Kellenbach, R. Boelens, R. Kaptein, Department of Chemistry, University of Utrecht, Padualaan 8, 3584 CH Utrecht, The Netherlands.
B. A. Maler, L. P. Freedman, K. R. Yamamoto, Department of Biochemistry and Biophysics, University of California at San Francisco, San Francisco, CA 94143–0448.
K. Dahlman, J. Carlstedt-Duke, J.-Å. Gustafsson, Department of Medical Nutrition and Center for Biotechnology, Karolinska Institute, Huddinge University Hospital, S-141 86 Huddinge, Sweden.

*On leave from Department of Medical Biophysics, Karolinska Institute, S-104 01 Stockholm, Sweden.
†Present address: Cell Biology and Genetics Program, Memorial Sloan-Kettering Cancer Center, New York, NY 10021.
‡To whom correspondence should be addressed.

several regions of extended peptide conformation. No evidence for α-helical domains could be found within the two finger regions. The identification of secondary structure elements also revealed that the pattern [finger-helix-extended region] is repeated twice within the DBD. Long-range NOEs resulting from protein folding can be found within and between these distinct regions (Fig. 2). For instance, NOEs are found within the two finger regions, between the two helical domains, between the first finger and the extended carboxyl-terminal region, as well as between the two finger regions.

The three-dimensional protein structure was determined with DG and distance bounds driven dynamics (DDD) (*12*) based on NOE connectivities, hydrogen bonds within identified secondary structure elements, and zinc atom coordination by Cys sulfurs. The structure determination is based on a set of 470 nonredundant NOE connectivities, including 194 sequential, 70 medium-range, and 134 long-range NOEs (*13*). The NOE intensities were converted to upper distance bounds with the use of initial NOE buildup rates obtained from NOESY spectra recorded with different mixing times (*14*) and calibrated versus known intraresidue and sequential proton-proton distances (*15*). The NOEs for which no reliable buildup curves could be obtained were assumed to represent a distance of ≤5 Å. Pseudoatom corrections were added for prochiral methylene groups, methyl groups, Phe and Tyr 2,6 and 3,5 ring protons, and Leu dimethyl groups (the eight Val methyl groups could be stereospecifically assigned) (*16*). Lower distance limits were in all cases taken as the sum of the van der Waals radii of the atoms or groups involved. The NOE constraints were supplemented by 18 amide-carbonyl hydrogen bonds (*17*) within secondary structure elements that could be identified from sequential NOE connectivities (two α helices, two reverse turns, and a short stretch of antiparallel β sheet).

Initial calculations showed that the DG structures could be further refined by including the effect of zinc coordination by conserved Cys residues. Tetrahedral zinc coordination was imposed by enforcing distance bounds of 3.83 ± 0.02 Å (*18*) between the sulfurs of Cys^{440}, Cys^{443}, Cys^{457}, and Cys^{460} in the first finger and Cys^{476}, Cys^{482}, Cys^{492}, and Cys^{495} in the second finger. The zinc coordination scheme within the second finger region has been the subject of some discussion, because this region contains five conserved Cys residues. However, site-directed mutagenesis studies clearly show that the conserved Cys^{500} can be replaced by Ala or Ser without significant loss of glucocorticoid receptor function and that this residue therefore cannot be involved in zinc complexation (*19*). This conclusion is strongly supported by recent studies of mutant DBD fragments in which each of the residues Cys^{492}, Cys^{495}, and Cys^{500} was replaced by Ser, showing that only Cys^{500} can be replaced without obstructing the protein folding (*20*). DG calculations that used tetrahedral zinc coordination within the second finger and excluded either Cys^{492}, Cys^{495}, or Cys^{500} yielded values of the DG error function that significantly favored the latter alternative (*21*). Zinc coordination involving residues Cys^{476}, Cys^{482}, Cys^{492}, and Cys^{495}, but not Cys^{500}, are therefore also consistent with NMR data.

Metric matrix DG was performed with an algorithm based on the original "embed" procedure (*22*), followed by 300 steps of conjugate gradient optimization of the DG constraint function (*12*). All DG structures were further subjected to 500 + 500 steps of DDD at 300 and 1 K, respectively, to obtain a more efficient sampling of "allowed" conformations (*23*). The DG calculations yielded protein structures with an average root-mean-square (rms) difference between peptide backbone atoms of 1.55 Å (Fig. 3). Structures that had been subjected to DDD showed somewhat larger rms differences (2.02 Å). The structure within a region forming a globular protein body (see below) is determined with a higher resolution (backbone rms differences of 1.32 Å after DG embedding and optimization and 1.52 Å after DDD). These data show that

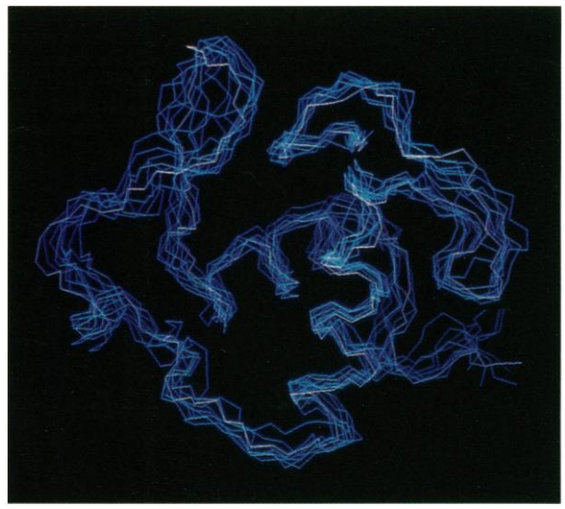

Fig. 3. Polypeptide backbone traces of a family of nine superimposed distance geometry structures for the glucocorticoid receptor DNA-binding domain (residues Cys^{440} to Arg^{510}). The view is approximately the same as in Fig. 4 (left).

Fig. 4. Ribbon model of the glucocorticoid receptor DNA-binding domain with two tetrahedrally coordinated zinc atoms. The view to the left is of the flat surface showing the protein body in the center with the first and second finger regions to the upper right and upper left, respectively. The view to the right is through the first helix (Ser^{459} to Glu^{469}), which is taken as a recognition helix in our model of the DBD-GRE complex (Fig. 5). The colors refer to the segments Cys^{440} to Gly^{470} (red) and Gln^{471} to Arg^{510} (green), including the first and second finger regions, respectively.

the present set of distance constraints is sufficient to describe the backbone folding of the DBD.

The DBD structure is shown in more detail in Fig. 4. The protein fragment has an overall oblate shape with long and short axis diameters of about 35 and 20 Å, respectively. One face is almost completely flat, whereas the other is in the shape of a cone. The two α helices are oriented perpendicular to each other, with hydrophilic surfaces exposed to the solvent. The α-helical regions and the extended peptide regions following each helix form a compact protein body. This body, which is better determined than the finger regions, is almost spherical with a diameter of about 20 Å. Several of the conserved hydrophobic residues, including Tyr[452], Phe[463], Phe[464], Val[468], His[472], Tyr[474], Tyr[497], Leu[501], Met[505], and Leu[508], form a hydrophobic core. The two zinc atoms are located outside the body, close to the flat surface, at a distance of about 13 Å from each other. The first finger domain is folded on top of the body and makes several contacts with the two helices and the carboxyl-terminal extended region. The second finger extends out from the body in two loops formed by the segments Ala[477] to Asp[481] and Ile[483] to Asn[491]. There are also contacts between the two finger domains, mainly involving residues Val[442] and Cys[443] and Asp[485] to Ile[487].

The structure of the DBD combined with genetic and biochemical data allow us to propose a model for the DBD-GRE complex. The recombinant DBD fragments studied here bind selectively to GRE DNA sequences that generally appear to consist of two half-site hexamers separated by three base pairs with a consensus sequence of GGTACANNNTGTTCT (where N is any nucleotide). A number of properties of the DBD-GRE complex were considered. First, DBD binds to the two GRE half-sites in a cooperative manner (*24*). Also, substitution of Ala[477] to Asp[481] with the corresponding segment of another receptor yields a protein that recognizes the GRE, but binds without cooperativity. Residues within this segment may therefore be determinants for protein-protein interactions in the dimeric complex (*25*). Second, three residues (458, 459, and 462) near the first zinc coordination site discriminate between glucocorticoid and estrogen response elements (*26*). Since the differences between the GRE and ERE (estrogen response element) can be found in the third and fourth base pairs of the two half-sites, it is conceivable that the three identified residues (or immediately adjacent amino acids) may actually contact these base pairs. Third, "missing base" contact and phosphate ethylation interference analyses show that the two DBD molecules interact with the major grooves of the GRE half-sites and that contacts are made with the corresponding phosphate groups located on the same face of the DNA (*27*).

A model of the DBD-GRE complex consistent with these observations is shown in Fig. 5. In this model, the α helix encompassing residues Ser[459] to Glu[469] is taken as a "recognition helix" located in the DNA major groove, with residues Gly[458], Ser[459], and Val[462] in close spatial proximity to the two middle AT base pairs of the GRE half sites. With this location, Lys[461], Lys[465], and Arg[466], which are conserved within the family of glucocorticoid, estrogen, and androgen receptors, can contact other bases within the GRE or the DNA phosphate backbone. The size and shape of the DBD makes it possible to orient the two monomers to form protein-protein contacts involving the segment that is important for cooperativity. Further features of this model include several favorable electrostatic interactions between charged Arg, Lys, and His residues and the DNA phosphates. Finally, we note that point mutants at positions 488, 489, and 491 within the second finger bind normally to GRE sequences but fail to enhance transcription in vivo (*28*); these "positive control" defects have been interpreted to define a region of the receptor that may contact components of the transcription machinery, thereby regulating initiation. In our model, amino acids in this region of the second finger extend away from the DNA and so are potentially available to interact with other proteins.

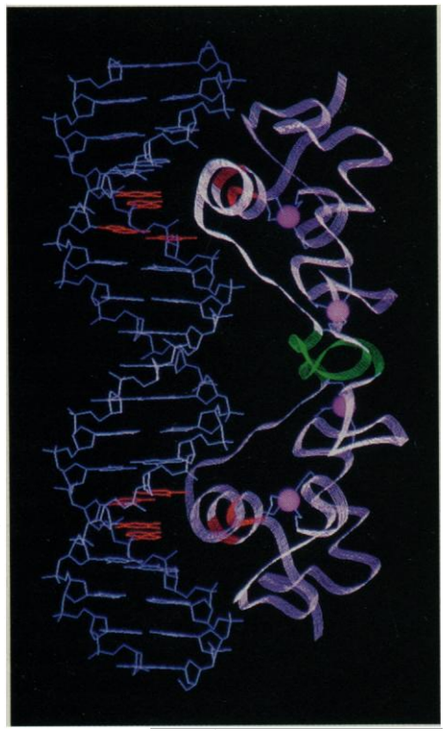

Fig. 5. Model of the dimeric complex between the glucocorticoid receptor DBD and the glucocorticoid response element (GRE). The GRE consensus sequence is 5′-NNGGTACANNNTGTTCT-NN-3′. The DBD residues essential for discrimination between glucocorticoid and estrogen response elements (GRE and ERE) (*26*) as well as two AT base pairs in the center of each of the GRE half-sites, indicating the differences between this GRE and the consensus ERE sequences, are colored in red. DBD residues in the segment that are important for protein-protein interactions (*25*) are colored in green.

We have presented a structure of the glucocorticoid receptor DBD and a model of the DBD-GRE complex that is consistent with experimental data. The DBD is folded in a single domain with several contacts between the two zinc finger regions, in contrast to the common view that the two zinc fingers should represent distinct subdomains. The structure of the steroid and thyroid hormone receptor fingers are significantly different from that of the TFIIIA type fingers (*29*). The large degree of sequence homology within the DBD between various members of the steroid and thyroid family of hormone receptors strongly suggests that the DBD structure of the other members of this family should be similar to the one we have presented.

REFERENCES AND NOTES

1. K. R. Yamamoto, *Annu. Rev. Genet.* **19**, 209 (1985); R. M. Evans, *Science* **240**, 889 (1988); M. Beato, *Cell* **56**, 335 (1989); J.-Å. Gustafsson *et al.*, *Endocrine Rev.* **8**, 185 (1987).
2. L. P. Freedman *et al.*, *Nature* **334**, 543 (1988).
3. K. Dahlman *et al.*, *J. Biol. Chem.* **264**, 804 (1989).
4. J. Miller, A. D. McLachlan, A. Klug, *EMBO J.* **4**, 1609 (1985).
5. L. M. Green and J. M. Berg, *Proc. Natl. Acad. Sci. U.S.A.* **86**, 4047 (1989).
6. J. M. Berg, *Cell* **57**, 1065 (1989).
7. The two protein fragments were KPARP(C440-G525)RL [numbering referring to the rat glucocorticoid receptor (*8*)], which was purified and checked for DNA-binding activity as described in (*2*), and S394-I519)RARYPGIL (numbering referring to the human glucocorticoid receptor), which was purified and checked for DNA-binding activity as described in (*3*). All sequence numbering in the text refers to the rat glucocorticoid receptor.
8. Abbreviations for the amino acid residues are A, Ala; C, Cys; D, Asp; E, Glu; F, Phe; G, Gly; H, His; I, Ile; K, Lys; L, Leu; M, Met; N, Asn; P, Pro; Q, Gln; R, Arg; S, Ser; T, Thr; V, Val; W, Trp; and Y, Tyr.
9. T. Härd *et al.*, *Biochemistry*, in press.
10. K. Wüthrich, in *NMR of Proteins and Nucleic Acids* (Wiley, New York, 1986).
11. S. W. Englander and A. J. Wand, *Biochemistry* **26**, 5953 (1987).
12. R. Kaptein, R. Boelens, R. M. Scheek, W. F. van Gunsteren, *ibid.* **27**, 5389 (1988); R. M. Scheek and R. Kaptein, in *Methods in Enzymology*, N. J. Oppenheimer and J. L. James, Eds. (Academic Press, New York, 1988).
13. Sequential NOEs refer to neighboring residues. Medium and long-range NOEs are here defined as connectivities between amino acids up to four residues apart, and five or more residues apart, respectively.
14. NOESY spectra [J. Jeener, B. H. Meier, P. Bach-

mann, R. R. Ernst, *J Chem. Phys.* **71**, 4546 (1979); D. J. States, R. A. Haberkorn, D. J. Ruben, *J Magn Reson.* **48**, 286 (1982)] were recorded at 300 K in 95:5 $^1H_2O/^2H_2O$ mixtures or 99.9% ^2H_2O in a buffer containing 300 mM NaCl, 0.1 mM NaN_3, and 1 mM phosphates at pH 6.5, with 1 mM DTE to prevent oxidation of cysteines. Spectra were recorded with mixing times of 10, 20, 40, and 80 ms ($^1H_2O/^2H_2O$) and 30, 60, 90, 120, and 150 ms (^2H_2O).

15. Buildup rates obtained in ^2H_2O were calibrated against Tyr2,6-Tyr3,5 NOEs (2.45 Å) Buildup rates in ^1H_2O involving NH protons were calibrated against the sequential NH_i-NH_{i+1} distance in α-helical regions [2.8 Å (*9*)]. Ten percent of the calculated distance, representing the experimental uncertainty, was added to the upper bound.
16. The pseudo-atom corrections were 1.0 Å for methylene and methyl groups, 1.5 Å for Leu dimethyl groups, and 2 Å for Phe and Tyr 3,5 and 2,6 protons.
17. Upper and lower distance bounds for the amide H and carbonyl O atoms were 2.3 and 1.85 Å, respectively.
18. Calculated for tetrahedral coordination assuming a Zn-S distance of 2.35 Å [L. Pauling, *The Chemical Bond* (Cornell Univ. Press, Ithaca, NY, 1967)].
19. Y. Severne, S. Wieland, W. Schaffner, S. Rusconi, *EMBO J.* 7, 2503 (1988).
20. J. Zilliacus, K. Dahlman-Wright, J. Carlstedt-Duke, J.-Å. Gustafsson, unpublished results.
21. Values of the DG error function (*14*) obtained for tetrahedral coordination of the sulfurs of Cys^{476} and Cys^{482} and two of the Cys^{492}, Cys^{495}, and Cys^{500} sulfurs were 153 ± 56, 200 ± 77, and 90 ± 62 $Å^4$ after DG embedding and optimization, and 72 ± 51, 98 ± 60, and 36 ± 35 $Å^4$ after DDD, when excluding Cys^{492}, Cys^{495}, or Cys^{500}, respectively.
22. T. F Havel, I. D. Kuntz, G. M. Crippen, *Bull Math. Biol.* **45**, 665 (1983); G. M. Crippen, *Distance Geometry and Conformational Calculations* (Wiley, New York, 1981).
23. DDD was run with a step size of 20 ps and a temperature coupling constant of 200 ps with a constraint force constant (*12*) of K_{dc} = 1 kJ mol^{-1} $Å^{-4}$.
24. T. Hard *et al.*, *Biochemistry* **29**, 5358 (1990).
25. K. Dahlman-Wright, A. Wright, J.-Å. Gustafsson, J. Carlstedt-Duke, unpublished results.
26. S. Mader, V. Kumar, H. de Verneuil, P. Chambon, *Nature* **338**, 271 (1989); K. Umesuno and R. M. Evans, *Cell* **57**, 1139 (1989); M. Danielsen, L. Hinck, G. M. Ringold, *ibid.*, p. 1131.
27. C. Cairns, J.-Å. Gustafsson, J. Carlstedt-Duke, unpublished results.
28. M. Schena, L. P. Freedman, K. R. Yamamoto, *Genes Dev.* **3**, 1590 (1989).
29. G. Párraga *et al.*, *Science* **241**, 1489 (1988); M. S. Lee, G. P. Gippert, K. V. Soman, D. A. Case, P. E. Wright, *ibid* **245**, 635 (1989).
30. Supported by the Netherlands Organization for Chemical Research (SON) and the Netherlands Organization of Scientific Research (NWO); 600-MHz ^1H NMR spectra were recorded at the national Dutch HF-NMR facility in Nijmegen with the assistance of S. Wymenga and J. Joordens. Additional financial support was obtained from the Swedish Medical Research Council (MFR), the Swedish National Board for Technical Development (to J.C.-D.), and NIH and NSF (grants to K.R.Y.). T.H. acknowledges a research fellowship from the Swedish National Research Council and financial support from the NWO. J.C.-D. acknowledges a research fellowship from MFR and K.D. acknowledges a predoctoral fellowship from MFR.

9 April 1990; accepted 10 May 1990

Methyl Chloride Transferase: A Carbocation Route for Biosynthesis of Halometabolites

ANNE MARIE WUOSMAA AND LOWELL P. HAGER

Enzymatic synthesis of methyl halides through an *S*-adenosyl methionine transfer mechanism has been detected in cell extracts of *Phellinus promaceus* (a white rot fungus), *Endocladia muricata* (a marine red algae), and *Mesembryanthemum crystallium* (ice plant). This mechanism represents a novel pathway for the formation of halometabolites. The Michaelis constants for chloride and bromide ion and for *S*-adenosyl methionine in the reaction have been determined for the enzyme from *E. muricata*. A recent survey of marine algae indicates that there may be a broad distribution of this enzyme among marine algae.

THE MOST ABUNDANT HALOHYDROcarbon species in the upper atmosphere is methyl chloride, and it is widely believed that biological synthesis is largely responsible for sustaining a global emission rate estimated to be 5×10^6 tons of methyl chloride per year (*1*). The synthesis of methyl chloride by cultures of wood rot fungi has been well documented (*2*), and there have been isolated studies reporting the in vivo synthesis of methyl halides by marine macroalgae and phytoplankton (*3*). However, in vitro methyl chloride synthesis has not been reported. The established enzymatic mechanism for the biosynthesis of halometabolites involves the hydrogen peroxide–dependent oxidation of halides to form electrophilic halogenating species (*4*). The electrophilic halogen intermediate generated in the peroxidase-reaction can react with a broad spectrum of nucleophilic acceptors to form the halometabolites. In our laboratory we demonstrated the synthesis of one prevalent atmospheric halohydrocarbon, methyltribromide, through the peroxidatic route (*5*). In the synthesis of this compound, bromoperoxidase first catalyzes the multiple bromination of an activated methylene carbon atom adjacent to a ketone function (*6*). The enzymatic bromination reaction is followed by the nonenzymatic hydrolysis of the tribrominated methyl group to release methyltribromide in a classical bromoform reaction. However, all of our attempts to detect monohalomethanes through chloro- or bromoperoxidase-type reactions have been unsuccessful. Thus we have recently turned our attention to a potential alternative route for the synthesis of methyl halides. White (*7*) has shown that when the fungus *Phellinus pomaceus* is grown on deuterium-labeled glucose, serine, or methionine, the methyl chloride produced is also labeled. This observation is consistent with the methyl chloride being derived from methionine. A likely route for this reaction would be through the methyl donor, *S*-adenosyl methionine. We report the detection and partial purification of a methyl transferase that catalyzes the methylation of chloride, bromide, and iodide ions.

Methyl chloride transferase activity has been detected in cell-free extracts prepared from the fungus *P. pomaceus*, from the ma-

Roger Adams Laboratory, Department of Biochemistry, University of Illinois, Urbana, IL 61801.

Table 1. Methyl transferase activity levels in whole cells and crude cell extracts. The activity measurements for fungal cells were obtained by growing cultures in 100 ml of 5% malt extract, 100 mM KCl, 1% bactopeptone liquid media in sealed bottles. Gas samples were removed each day and analyzed as described in Fig. 1. Known amounts of methyl chloride in identically prepared bottles were used as standards. The value reported here was the amount of methyl chloride obtained during peak production periods. The values for whole cells of *E. muricata* and *M. crystallium* were obtained by incubating whole cells in 100 mM KCl in gas-tight vials. Gas samples were analyzed as in Fig. 1 with known amounts of methyl chloride as standards. The values for all crude cell extracts were obtained by incubating the cell extracts in 4-ml reaction mixtures containing 250 mM KCl, 500 μM SAM, 100 mM phosphate, pH 6.8. The *P. pomaceus* cell extracts were obtained by digesting cells with 10 mg of Novozyme 234 per milliliter for 1 hour followed by removal of cell debris by centrifugation. Cell extracts of *E. muricata* were obtained as in Fig. 1. Cell extracts of *M. crystallium* were obtained by grinding the cells in a Waring blender. Gas samples were analyzed in the same manner as those from whole cells.

Source	Methyl chloride production	
	Whole cells (pmol g^{-1} day^{-1})	Crude extract (fmol min^{-1} mg^{-1})
P. pomaceus	7	25
E. muricata	30	670
M. crystallium	19	3